

Enhanced Aerosol Estimations From Suomi-NPP VIIRS Images Over Heterogeneous Surfaces

Jing Wei^{ID}, Student Member, IEEE, Zhanqing Li^{ID}, Lin Sun^{ID}, Yikun Yang, Chuanfeng Zhao, and Zhaoxin Cai

Abstract—The Visible Infrared Imaging Radiometer Suite (VIIRS) on board the Suomi National Polar-orbiting Partnership (NPP) is a new-generation polar-orbiting satellite imaging sensor. It has generated a variety of operational products similar to the widely used Moderate Resolution Imaging Spectroradiometer (MODIS) products. However, there are high uncertainties in official VIIRS aerosol products based on our previous validations, and a reduction in these uncertainties is needed before they can be used with confidence. To this end, we developed a revised high-spatial-resolution aerosol retrieval algorithm which can considerably improve the aerosol optical depth (AOD) estimations. The improvements mainly arise from: 1) correction of the surface bidirectional reflectance using the Ross-Thick-LiSparse model with parameters obtained from the MODIS bidirectional reflectance distribution function (BRDF)/Albedo products; 2) finer customized monthly aerosol types assumed from the historical Aerosol Robotic Network (AERONET) measurements of optical properties; and 3) improved cloud screening with the revised dynamic threshold cloud detection algorithm. The new 750-m AOD retrievals are validated against AERONET AOD measurements and compared with the official VIIRS AOD products from 2014 to 2017 over the Beijing-Tianjin-Hebei region in China. The results illustrated that the retrievals are highly consistent with ground measurements ($R = 0.926$), with ~72% of them falling within the expected error of [$\pm(0.05 + 20\%)$] on a regional scale. The mean absolute error is 0.082 and the root-mean-square error is 0.120. The new algorithm can significantly reduce the overestimations and improve the aerosol estimations over heterogeneous urban surfaces compared to the official aerosol products, especially in winter. This new VIIRS AOD product will thus be more useful for air pollution studies over medium- or small-scale areas.

Index Terms—Aerosol optical depth (AOD), Aerosol Robotic Network (AERONET), bidirectional reflectance distribution

Manuscript received January 31, 2019; revised May 19, 2019; accepted June 20, 2019. Date of publication August 1, 2019; date of current version November 25, 2019. This work was supported in part by the National Key Research and Development Program of China under Grant 2017YFC1501702, in part by the National Natural Science Foundation of China under Grant 91544217, in part by the U.S. National Science Foundation under Grant AGS1534670 and Grant AGS1837811, and in part by the BNU Interdisciplinary Research Foundation for the First-Year Doctoral Candidates under Grant BNUXKJC1808. (Corresponding author: Zhanqing Li.)

J. Wei, Y. Yang, C. Zhao, and Z. Cai are with the State Key Laboratory of Remote Sensing Science, College of Global Change and Earth System Science, Beijing Normal University, Beijing 100875, China (e-mail: weijing_rs@163.com; ykyang@mail.bnu.edu.cn; czhao@bnu.edu.cn; caizhaoxin1234@163.com).

Z. Li is with the Department of Atmospheric and Oceanic Science, Earth System Science Interdisciplinary Center, University of Maryland, College Park, MD 20740 USA (e-mail: zli@atmos.umd.edu).

L. Sun is with the College of Geomatics, Shandong University of Science and Technology, Qingdao 266590, China (e-mail: sunlin6@126.com).

Color versions of one or more of the figures in this article are available online at <http://ieeexplore.ieee.org>.

Digital Object Identifier 10.1109/TGRS.2019.2927432

function (BRDF), Visible Infrared Imaging Radiometer Suite (VIIRS).

I. INTRODUCTION

A TMOSPHERIC aerosols can directly or indirectly affect the earth's surface by scattering and absorbing solar radiation [1], [2]. They can play important roles in climate change, the atmospheric environment, air pollution, and human health [3]–[8]. The aerosol optical depth (AOD) is the most fundamental quantity denoting aerosol loading and is described by the attenuation of light by aerosol particles. It has been involved in various aspects of atmospheric studies including aerosol–cloud–precipitation interactions, model simulations, and near-surface particulate matter estimations [9]–[12].

In the modern era of earth observation, global-coverage aerosol products have been generated from the Moderate Resolution Imaging Spectroradiometer (MODIS) since 1999 and the Visible Infrared Imaging Radiometer Suite (VIIRS) since 2011. The MODIS and VIIRS aerosol products are compatible because they employ heritage algorithms previously applied to similar sensors. They have provided multi-decade AOD records together, which are thus most useful for exploring the long-term climate and environmental changes from regional to global scales. Moreover, for regional applications, efforts have been made to improve the aerosol estimations from instruments on different satellite platforms, e.g., Landsat [13], [14], MODIS [15]–[18], and Himawari Imager [19]–[21].

The VIIRS aerosol retrieval algorithm has also been revised and assessed on regional or global scales. A revised VIIRS aerosol retrieval algorithm is developed using a precalculated and atmosphere-corrected global surface reflectance ratio database at a resolution of 0.1° over dark and bright surfaces [22]. The 6-km-resolution VIIRS AOD retrievals are overall improved than the official products compared with Aerosol Robotic Network (AERONET) AOD measurements. The SeaWiFS Ocean Aerosol Retrieval algorithm is extended to be applied for VIIRS images over water bodies with several advancements (e.g., the surface reflectance model and the aggregation procedure) at a 6-km spatial resolution [23]. The retrieved AOD, the Ångström exponent, and the fine-mode AOD fractions agree well with the Maritime Aerosol Network measurements. A new aerosol retrieval algorithm is proposed which synergistically used Terra, Aqua MODIS, and VIIRS single-data records to derive atmosphere-surface properties at a 3-km spatial resolution over Eastern China [24]. The retrievals

TABLE I
CHARACTERISTICS OF THE AQUA-MODIS AND VIIRS SENSORS

Characteristics	Aqua-MODIS	VIIRS
Launch time	May 2002	October 2011
Orbit altitude	705 km	824 km
Imaging time	13:30 LT	13:30 LT
Swath width	2330 km	3040 km
Solar zenith angle	< 82°	< 82°
Solar zenith angle	±64°	±70°
Spectral channels	36	22
Central wavelength	0.41, 0.47, 0.65, 0.86, 1.24, 2.11, 11, 12 μm	0.41, 0.49, 0.67, 0.87, 1.24, 2.25, 11, 12 μm
Spatial resolution	250 m, 500 m, 1000 m	375 m and 750 m
Temporal resolution	Each day	Each day
Bow-tie effects	Yes	No

are overall better than MODIS and VIIRS official products compared with surface measurements.

Numerous studies have reported problems with the current official VIIRS aerosol products associated with the estimation of surface reflectance and preassigned aerosol types in China, especially for the Beijing–Tianjin–Hebei and Yangtze River Delta regions with complex aerosol properties and heterogeneous surfaces [25]–[28]. Meanwhile, the relatively coarse spatial resolution (6 km) can severely limit their applications on small scales, especially in urban areas. Therefore, this study aims to revise the current aerosol algorithm for improving aerosol retrievals in terms of both accuracy and spatial resolution over land. For this, several main challenges having to do with aerosol remote sensing are tackled including the estimation of surface reflectance, assumption of aerosol types, and cloud screening [29]. The merits of the improvements over the Beijing–Tianjin–Hebei region in Eastern China from 2014 to 2017 are demonstrated.

II. DATA SOURCES

A. VIIRS Data Records

VIIRS acquires daily records at five high-spatial-resolution (375 m) channels and 16 moderate-spatial-resolution (750 m) channels, and one independent day/night channel, covering the wavelengths from 0.41 to 12.5 μm. The swath width is 3040 km and the imaging time is ~13:30 local equator crossing time [30], [31]. Table I provides the main characteristics of the Aqua-MODIS and VIIRS sensors.

The VIIRS daily aerosol product (VAOOO) is one of a series of atmospheric Level 2 environmental data records (EDR). It is generated by a modified dark target (DT) aerosol retrieval algorithm [30]. The surface reflectances for the blue (M3) and red (M5) channels are estimated by virtue of their empirical relationships with that in the shortwave infrared (SWIR, M11) channel ($M11/M5 = 1.788$, $M3/M5 = 0.645$). Three over-land aerosol models including dust, low/high-absorption smoke, and clean/polluted urban were assigned based on geographic zones. The DT algorithm is only valid

for cloud-free dark surfaces. Unsuitable pixels (i.e., clouds, snow/ice, and bright surfaces) are screening using the official VIIRS Cloud Mask (VCM) algorithm. AOD is then derived from the precalculated look-up-table (LUT) at the original 750 m and then averaged (8*8 retrievals) to a coarser spatial resolution of 6 km. The AOD retrievals are reported at several wavelengths and divided into three data-quality levels using quality assurance (QA): Low (QA = 1), Medium (QA = 2), and High (QA = 3). The VAOOO AOD products with high-quality retrievals (QA = 3) at 550 nm from 2014 to 2017 are collected and used for comparison in this study [28], [30].

B. AERONET Ground Measurements

AERONET is a ground-based aerosol network that provides worldwide freely available ground measurements of aerosol optical properties. The spectral AODs are reported at visible to near-infrared independent wavelengths every 15 min with a low bias of ~0.01–0.02 under cloud-free conditions. The AOD measurements include three levels: Level 1.0 (unscreened), Level 1.5 (cloud-screened), and Level 2.0 (cloud-screened and quality-assured). The data version was updated from Version 2 to Version 3 in January 2018, with further cloud screening and quality control [32], [33]. Thus, the AERONET Version 3 AOD measurements are selected in this study, and the Level 1.5 data are used only if Level 2.0 data were not available due to a limited number of sites in the study area. We employed AERONET data at six ground sites including four urban sites and two vegetated sites in the Beijing–Tianjin–Hebei region. Historical monthly aerosol optical properties [e.g., the single-scattering albedo (SSA), asymmetry factor (g), and complex refractive index (CRI)] from 2008 to 2017 are selected to help more accurately determine aerosol characteristics in the study area. Instantaneous AOD observations from 2014 to 2017 are collected to verify the aerosol retrievals in this study.

III. METHODOLOGY

The revised VIIRS aerosol algorithm developed in this paper is partly based on our previously proposed, regionally robust high-spatial-resolution aerosol (RRHA) retrieval algorithm [18], but is an extension with a series of improvements made to address three key challenges in aerosol remote sensing, including: 1) modified VIIRS surface bidirectional reflectance; 2) improved assumption of finer monthly aerosol models; and 3) updated dynamic threshold cloud detection algorithm for VIIRS images. The atmospheric radiative transfer model can be expressed conceptually as follows:

$$\rho^* = T_{\text{og}} T_{\text{O}_3} \left[\rho_{\text{Aer}} T_{\text{H}_2\text{O}} \left(\frac{C_{\text{H}_2\text{O}}}{2} \right) + \rho_{\text{Ray}} + T_{\text{H}_2\text{O}} (C_{\text{H}_2\text{O}}) T_{\theta_s} T_{\theta_b} \frac{\rho_s}{1 - \rho_s S_{\lambda}} \right] \quad (1)$$

where ρ^* is the top-of-atmosphere (TOA) reflectance; ρ_{Aer} and ρ_{Ray} are the atmospheric intrinsic reflectances due to aerosol scattering and Rayleigh scattering, respectively; $T_{\text{H}_2\text{O}}$, T_{O_3} , and T_{og} are the two-way transmittances for total water vapor (H_2O), ozone (O_3), and other gases (e.g., CO_2 , O_2 , and CH_4); $C_{\text{H}_2\text{O}}$ represents the total column amount of water

vapor in the atmosphere (unit: cm); θ_s and θ_v represent the solar zenith angle and the satellite zenith angle; T_{θ_s} and T_{θ_v} represent the atmospheric transmissions; S is the atmospheric spherical albedo; and ρ_s is the surface reflectance.

In (1), the Rayleigh intrinsic reflectance for actual pressure (obtained from European Centre for Medium-Range Weather Forecasts (ECWMF) Re-Analysis (ERA)-Interim daily pressure measurements) is done by adjusting the molecular optical depth [17]. Note that the added Rayleigh scattering correction is indeed for nonabsorbing aerosol under low aerosol loading conditions, but is limited for absorbing aerosol cases for all optical depth situations. The gas transmissions for H_2O , O_3 , and other gases at a given wavelength (λ) are calculated based on updated empirical approximations [18]. The remaining three main improvements in surface reflectance, aerosol type, and cloud detection are described in detail below.

A. Modified Surface Reflectance Estimation

Surface reflectance is one of the crucial factors affecting aerosol retrieval accuracy. Fig. 1(a) shows the simulated aerosol changes to VIIRS TOA reflectances (at $0.49 \mu\text{m}$) under varying surface reflectances ranging from 0.01 to 0.10 (i.e., from dark to bright surfaces). The result shows a strong roughly linear relationship between TOA reflectances and AODs. The sensitivity of aerosol changes to TOA reflectances decreases gradually with increasing surface reflectance, suggesting an increasing difficulty in aerosol retrieval over bright surfaces. In general, a 1% estimation error in surface reflectance can lead to about $\sim 10\%$ retrieval error under highly polluted conditions. However, under less polluted conditions, the retrieval error can increase by more than 20% with the same 1% estimation error. Similar results have also been reported for Landsat and MODIS data [13], [28].

Therefore, the daily surface reflectance is calculated and used in this study to reduce the estimation error rather than the coarser temporal resolutions (i.e., seasonal, monthly, and eight days) used in previous studies [13]–[17], [21], [39]. Meanwhile, the use of surface bidirectional reflectance can effectively minimize the effects of the surface bidirectional reflectance distribution function (BRDF) over high heterogeneous surfaces [18]. Therefore, the reciprocal combination of the RossThick model and the LiSparse model is selected to calculate the daily surface bidirectional reflectance. Due to different geometric conditions between MODIS and VIIRS sensors, the MODIS BRDF-Albedo Model Parameters Product (MCD43A1) at a high spatial resolution of 500 m is selected to provide the weighted coefficients of the isotropic-scattering, volume-scattering, and surface-scattering kernels [34]. These parameters are resampled to 750 m using the bidirectional linear interpolation method, and the daily surface bidirectional reflectance is calculated based on their geometric information using the RossThick-LiSparse model for VIIRS images [35]–[38].

B. Finer Aerosol-Type Assumption

Due to constantly changing aerosol composition over land, the aerosol model is another key factor affecting aerosol

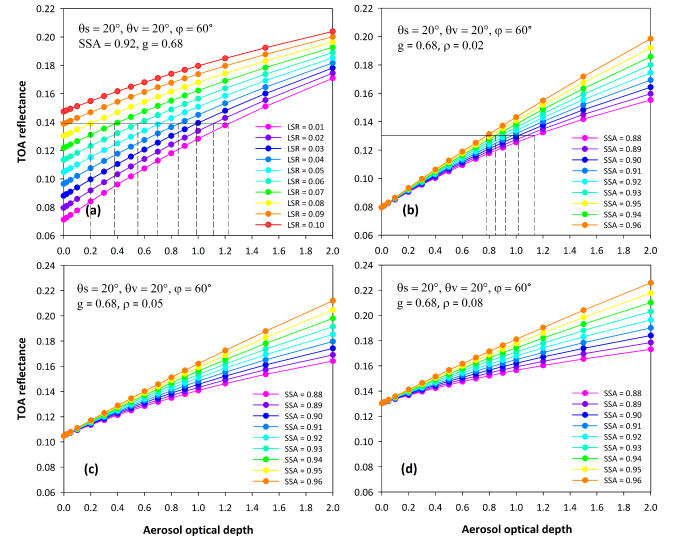


Fig. 1. Sensitivity of aerosol changes to VIIRS TOA reflectances ($0.49 \mu\text{m}$) as a function of (a) land surface reflectance (LSR) and (b)–(d) aerosol type (represented by SSA) over land. The viewing geometry is the same in all panels ($\theta_s = 20^\circ$, $\theta_v = 20^\circ$, and $\varphi = 60^\circ$), where SSA, g , and φ represent the single scattering albedo, the asymmetry factor, and the relative azimuth angle, respectively.

retrieval accuracy. The SSA (ω) is one of the main parameters determining the aerosol type over land. Fig. 1(b)–(d) show the simulated relationships between TOA reflectance and AOD with varying SSA values ranging from 0.88 (strongly absorbing) to 0.96 (almost no absorption) under different surface conditions. Under highly polluted conditions, a 1% estimation error in the SSA can lead to $\sim 5\%$ retrieval errors. These retrieval errors get larger as air pollution increases. Meanwhile, the retrieval errors become larger as the surface reflectance increases.

For the official VIIRS modified DT [30], MODIS DT [39], and Deep Blue [40] aerosol algorithms, only several zonal fixed aerosol types are defined through cluster analysis with AERONET climatology on a global scale. This is inappropriate for local or specific areas. Therefore, we have examined the changes in optical properties of aerosols using the time series analysis with the historical monthly *in situ* AERONET measurements in the study area. Our previous study found that the main monthly aerosol optical properties are more stable in interannual years, but with obvious seasonal variations in aerosol compositions. Four seasonal aerosol types were thus assumed for use in aerosol retrievals [14], [18]. However, there are still nonnegligible differences in the main aerosol optical properties among the months over the year (Fig. 1 in [18]). Different from our previous study, to more accurately determine aerosol compositions in the study area, more detailed monthly rather than seasonal aerosol models are first assumed for aerosol retrieval in the study.

For this, three main aerosol optical properties (i.e., SSA, g , and the CRI) during 2008–2017 are thus averaged for each month using the updated AERONET Version 3 monthly measurements, and 12 finer monthly aerosol models are defined in the study area (Table II). The results show that the SSA

TABLE II
OPTICAL PROPERTIES OF FOUR CUSTOM SEASONAL AEROSOL MODELS USED IN AOD RETRIEVAL

Model	SSA (0.49/0.55/0.67μm)	g (0.49/0.55/0.67μm)	RP-CRI (0.49/0.55/0.67μm)	IP-CRI (0.49/0.55/0.67μm)
January	0.886/0.889/0.892	0.704/0.677/0.653	1.535/1.540/1.545	0.017/0.015/0.014
February	0.900/0.904/0.906	0.700/0.674/0.651	1.528/1.534/1.539	0.013/0.011/0.010
March	0.913/0.919/0.925	0.705/0.680/0.657	1.528/1.536/1.543	0.010/0.008/0.008
April	0.922/0.927/0.935	0.711/0.687/0.666	1.518/1.527/1.534	0.008/0.007/0.006
May	0.925/0.930/0.937	0.713/0.687/0.663	1.516/1.524/1.531	0.007/0.006/0.005
June	0.947/0.948/0.947	0.716/0.687/0.661	1.478/1.481/1.483	0.006/0.006/0.005
July	0.955/0.955/0.954	0.725/0.700/0.677	1.465/1.465/1.466	0.006/0.006/0.006
August	0.944/0.944/0.942	0.717/0.692/0.670	1.490/1.490/1.491	0.008/0.008/0.008
September	0.923/0.923/0.921	0.713/0.687/0.665	1.514/1.516/1.517	0.012/0.010/0.010
October	0.916/0.919/0.921	0.712/0.688/0.666	1.520/1.520/1.520	0.013/0.011/0.011
November	0.890/0.895/0.897	0.701/0.675/0.651	1.526/1.532/1.537	0.015/0.013/0.012
December	0.881/0.887/0.891	0.707/0.680/0.657	1.536/1.543/1.551	0.018/0.015/0.015

ranges from 0.88 to 0.96 in the study area, suggesting significant changes in aerosol characteristics within a year. SSA reaches the maximum value of 0.954 in July and a minimum value of 0.891 in December. Similar changes are seen in g , i.e., the maximum value in July and the minimum value in February. However, the real (RP) and imaginary (IP) parts of the CRI show opposite variations where the maximum and minimum values are observed in December and July, respectively.

C. Updated Unusable Pixel Screening

For cloud pixels, the universal dynamic threshold cloud detection algorithm (UDTCDA), which has strong ability to detect different kinds of cloud types (especially for thick and thin clouds) over varying underlying surfaces, is selected in this study [41]. Therefore, the dynamic-threshold models from visible to near-infrared channels for the VIIRS sensor are resimulated and constructed under different geometrically observed and atmospheric conditions as follows:

$$\rho_b^{*'} = 0.802 * \rho_b + 0.034 * \cos \theta_s \cos \theta_v + 0.161 \quad (2)$$

$$\rho_g^{*'} = 0.804 * \rho_g + 0.022 * \cos \theta_s \cos \theta_v + 0.139 \quad (3)$$

$$\rho_r^{*'} = 0.877 * \rho_r + 0.013 * \cos \theta_s \cos \theta_v + 0.123 \quad (4)$$

$$\rho_{\text{NIR}}^{*'} = 0.914 * \rho_{\text{NIR}} + 0.006 * \cos \theta_s \cos \theta_v + 0.111 \quad (5)$$

$$C_i = \rho_i^* > \rho_i^{*'} \text{ and Final} = C_b \cup C_g \cup C_r \cup C_{\text{NIR}} \quad (6)$$

where $\rho_i^{*'}$ represents the dynamic cloud thresholds at the blue ($\rho_b^{*'}$), green ($\rho_g^{*'}$), red ($\rho_r^{*'}$), and NIR ($\rho_{\text{NIR}}^{*'}$) channels. C_i represents the channel-dependent cloud result and Final represents the final cloud mask. ρ_i represents the surface reflectance. However, despite high similarities, the differences in the spectral response functions between the two sensors need to be corrected when using the prior MODIS surface reflectance database for support. For this, 1200 measured spectra (400–2500 nm) at a spectral resolution of 1-nm covering most features are collected from multi-source spectral libraries [41]. The surface reflectances are computed using

satellite-specific filter response functions and converted with the linear relationships at different wavelengths [42].

To help improve the cloud detection results for thin clouds over bright surfaces, the TOA reflectance in the blue channel (R_{M3}), the brightness temperature (BT_{M15}), and the BT differences (BTD) between M15 and M16 are also involved:

$$R_{M3} < 0.40 \cap BT_{M15} < 285 \quad (7)$$

$$R_{M3} > 0.15 \cap BT_{M15} < 280 \cap BTD > 1.8. \quad (8)$$

Potential snow and ice surfaces are identified using the normalized difference snow index (NDSI), BT_{M15} , and the TOA reflectance in band 7 (R_{M7}):

$$NDSI < 0.4 \cap BT_{M15} < 280 \cap R_{M7} < 0.21. \quad (9)$$

D. Aerosol Retrieval

The LUT approach is selected for aerosol retrieval in this study. The LUTs for different aerosol models at different wavelengths are precalculated using the second simulation of the satellite signal in the solar spectrum (6S) model under different atmospheric, surface, and geometric conditions. Pixels passing all the unusable pixel screening tests are masked during the aerosol retrieval. Finally, a spatial homogeneity filter with a 3×3 running average window is applied to the final 750-m-resolution results to minimize the effects of salt-and-pepper noise. Table III summarizes the differences in the official and our revised aerosol algorithms.

E. Evaluation Approaches

AERONET Version 3 AOD measurements and VAOOO AOD products are collected for validation and comparison purposes. AOD retrievals within a sampling window (5×5 pixels) around a ground site from the satellite-derived aerosol data set are averaged. AERONET AODs at each site (at least two observations) within ± 30 min of VIIRS overpass time are averaged to obtain a temporally matched AOD. The 550-nm AODs are interpolated using the Ångström exponent

TABLE III
DIFFERENCE BETWEEN VIIRS AEROSOL RETRIEVAL ALGORITHMS

Parameters	Official VIIRS algorithm	Revised VIIRS algorithm
Channel	0.41, 0.49, 0.67, 2.25	0.49, 0.67
Gas absorption	Empirical relationships	Improved approximations
Surface reflectance	Surface reflectance (constant empirical reflectance ratios)	Surface bidirectional reflectance (RossThick-LiSparse model)
Aerosol model	Five global empirical zone aerosol types	Twelve regional monthly aerosol types
Cloud detection	VCM algorithm	UDTCDA algorithm
Spatial resolution	6 km	750 m
AOD	550 nm	550 nm
AOD range	[0, 2]	[0, 3]

algorithm in the 440–675 nm range due to the absence of 550-nm observations. The accuracy and uncertainty are reported based on the number of matched retrievals (N), the correlation coefficient (R), the mean absolute error (MAE), the root-mean-square error (RMSE), the relative mean bias (RMB), the expected error (EE, $\pm[0.05 + 20\%]$) over land, and the relative difference [43].

IV. RESULTS AND DISCUSSION

A. Validation Against AERONET AOD Measurements

1) *Validation on Site and Regional Scales:* The AOD retrievals are validated against AERONET ground-based measurements from 2014 to 2017 on the site and regional scales (Table IV). There are 349, 356, and 284 matchups collected at the Beijing, Beijing-CAMS, and Beijing_RADI sites, but fewer matchups at the Beijing_PKU site due to shorter operation time. VIIRS AOD retrievals agree well with AERONET AODs with high correlations ($R = 0.91$ –0.94) and about 69%, 65%, 80%, and 70% of them falling within the EE envelope at above four sites, respectively. The estimation uncertainties are generally low over urban with average MAE and RMSE values less than 0.09 and 0.13, and RMB values close to 1.

Xianghe and Xinglong are two typical vegetated sites close to croplands in the suburban areas of the study area. There are 369 matchups at the Xianghe site, and they correlated well with surface observations ($R = 0.922$). Approximately, 75% of the matched retrievals fall within the EE envelope with an average MAE of 0.089 and an RMSE of 0.140. Less than 3% of the retrievals is overestimated. The Xinglong site ceased operation at the end of 2014, so only one-year retrievals were available, and approximately 83% of the matchups fall within the EE envelope with low estimation uncertainties.

On the regional scale, a total of 1539 collected matchups agree well with ground observations ($R = 0.926$). The average MAE and RMSE values are 0.082 and 0.120, with ~13% overestimations. In general, ~72% of the matchups fall within the EE envelope. These results illustrate that the revised algorithm works well over both bright urban and dark vegetated surfaces.

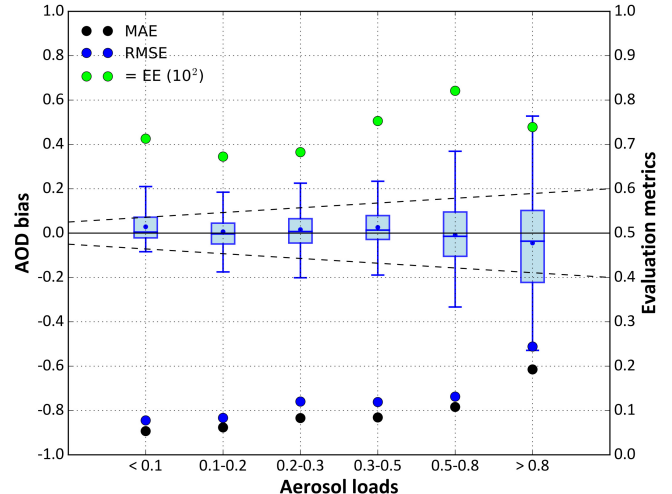


Fig. 2. Bias box plots and performance of VIIRS AOD retrievals (750 m) as a function of aerosol loading from 2014 to 2017. The dotted lines represent the EE envelope, respectively.

2) *Performance Related to Aerosol Loads:* Fig. 2 shows box plots and the performance of VIIRS (750-m resolution) AOD retrievals as a function of aerosol loading in the study area from 2014 to 2017. For low aerosol loadings ($AOD < 0.5$), more than 67% of AOD retrievals fall within the EE envelope, showing small estimation uncertainties (MAE < 0.08 and RMSE < 0.12) but with positive biases, especially for $AOD \leq 0.1$. Because the same estimation error in surface reflectance under low aerosol loadings can lead to large retrieval errors than under high aerosol loadings. Under moderately to highly polluted conditions ($AOD > 0.5$), an increasing percentage of more than 74% of retrievals fall within the EE envelope. However, the estimation uncertainty becomes large with increasing MAE and RMSE values, and the biases become more negative as AOD increases. Although the retrievals worsen as the aerosol loading increases, the revised algorithm performs well overall under different aerosol loading conditions.

B. Comparison With Official VIIRS AOD Products

1) *Comparison on Site and Regional Scales:* Fig. 3 shows the comparisons between our 750-m and official 6-km AOD retrievals against AERONET ground measurements. Table IV also gives the site-scale validation of VAOOO AODs in the study area. Compared to the official VIIRS AOD product, the number of matched samples generated from our algorithm significantly increases by about 76%, 50%, 68%, and 52% for Beijing, Beijing-CAMS, Beijing_RADI, and Beijing_PKU sites, respectively. VAOOO AOD retrievals show large estimation uncertainty at each urban site with MAEs and RMSEs greater than 0.22 and 0.29. They significantly overestimate the aerosol loading with more than 54% of the matched retrievals falling above the upper boundary of the EE envelope. By contrast, our AOD retrievals are improved with higher correlations and smaller biases close to zero at each site than the official AODs. In addition, the fractions of matchups within

TABLE IV
VALIDATION OF VIIRS AOD RETRIEVALS AT EACH SITE IN THE STUDY AREA. DATA ARE FROM 2014 TO 2017

Site	N		R		MAE		RMSE		RMB		Within EE (%)		Above EE (%)	EE (%)
	New	VAOOO	VAOOO	New	VAOOO	New	VAOOO	New	VAOOO	New	VAOOO	New	VAOOO	VAOOO
Beijing	349	198	0.927	0.722	0.084	0.235	0.117	0.323	1.046	1.438	69.05	36.87	20.63	59.09
Beijing-CAMS	356	237	0.918	0.751	0.088	0.241	0.123	0.318	1.061	1.497	64.89	34.60	23.03	59.92
Beijing_RADI	284	169	0.931	0.674	0.070	0.235	0.105	0.331	1.051	1.567	79.58	37.28	14.44	59.17
Beijing_PKU	128	84	0.939	0.856	0.080	0.224	0.109	0.293	0.927	1.260	70.31	38.10	07.03	53.57
Xianghe	369	227	0.922	0.869	0.089	0.134	0.140	0.230	1.025	0.894	74.80	70.93	18.43	09.25
Xinglong	53	42	0.952	0.959	0.052	0.059	0.069	0.080	0.881	0.935	83.02	80.95	05.66	02.38
All sites	1539	957	0.926	0.759	0.082	0.204	0.120	0.294	1.128	1.279	71.99	46.50	17.87	44.51

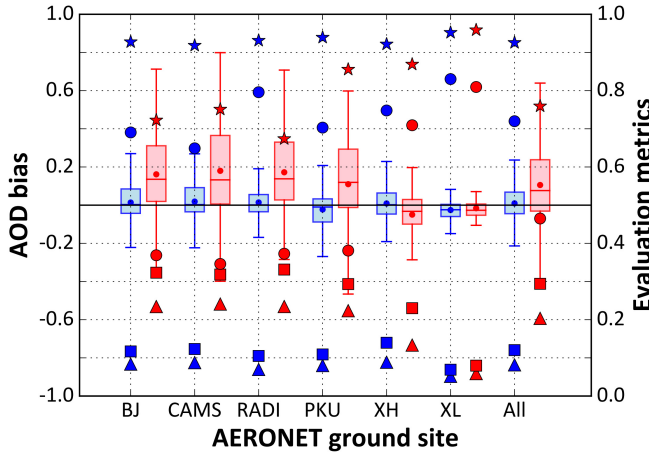


Fig. 3. Validation and comparison of our new 750-m AOD retrievals (in blue) and VAOOO 6-km AOD retrievals (in red) against AERONET AODs from 2014 to 2017 at each site in the study area. Stars, filled circles, triangles, and squares represent the correlation (R), within EE (10^2), MAE, and RMSE (right-hand y-axis), where BJ, XH, and XL represent the Beijing, Xianghe, and Xinglong sites (x-axis), respectively.

the EE envelope increase by approximately 32%, 30%, 40%, and 32%, and the estimation uncertainties are significantly reduced in MAEs by 64%, 65%, 70%, and 64%, and in RMSEs by 64%, 61%, 68%, and 63% for four sites, respectively.

For two vegetated sites, the VAOOO AOD retrievals are improved with small negative biases, low estimation uncertainties (MAE = 0.06–0.14 and RMSE = 0.08–0.23), and approximately twice more matched retrievals falling within the EE envelope (~70%–81%) than for the urban sites. In general, our new AOD retrievals increase the number of matched retrievals by 63% and 26% at the XiangHe and Xinglong sites, respectively, compared to VAOOO AODs. The fraction of matchups falling within the EE envelope increases by ~3%–4%, and the MAE and RMSE values decrease by 12%–34% and 13%–40%, respectively.

On a regional scale, there are 957 matched retrievals between VAOOO and AERONET AODs from six sites. The two retrievals agree well ($R = 0.759$), but have a large estimation uncertainty (MAE = 0.204 and RMSE = 0.294). Approximately, 47% and 45% of the matchups are within

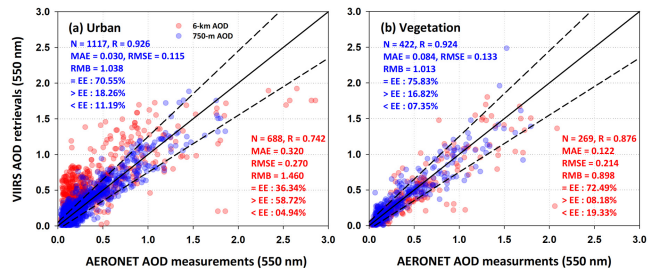


Fig. 4. Scatterplots of new 750-m AOD retrievals (blue dots) matched with VAOOO 6-km AOD retrievals (red dots) against AERONET AOD measurements from 2014 to 2017 over (a) urban and (b) vegetated surfaces.

and above the upper boundary of the EE envelope, indicating an overall poor performance of the official AOD product. By contrast, our new algorithm can significantly improve the aerosol estimations with approximately 61% more successful retrievals, and largely decreasing MAE and RMSE values by 60% and 59%, respectively. There are ~25% more data samples falling within the EE envelope with greatly reduced overestimations. These results illustrate that the new AOD data set is improved and less biased than the official AOD product on both site and regional scales.

2) Comparison Over Different Land Use Types: This section compares the overall performance between the two aerosol data sets over two urban (including the Beijing, Beijing-CAMS, Beijing_RADI and Beijing_PKU sites) and vegetation (including the Xianghe and Xinglong sites) surfaces (Fig. 4). Over the urban area, the VAOOO AODs ($N = 688$) agree poorly with AERONET ground measurements ($R = 0.742$) with an average MAE of 0.320 and an RMSE of 0.270 [Fig. 4(a)]. In general, 36% and 59% of the retrievals fall within and above the upper boundary of the EE envelope, indicating significant overestimations (RMB = 1.460). By contrast, our algorithm generates 62% more successful retrievals ($N = 1117$) that agree better with ground-measurements ($R = 0.926$) with a much lower MAE of 0.03 and an RMSE of 0.115. The fraction of matched retrievals within the EE envelope is 71%, which is almost twice more than that of the VAOOO AOD product, significantly reducing the overestimations. These results illustrated that our revised algorithm works

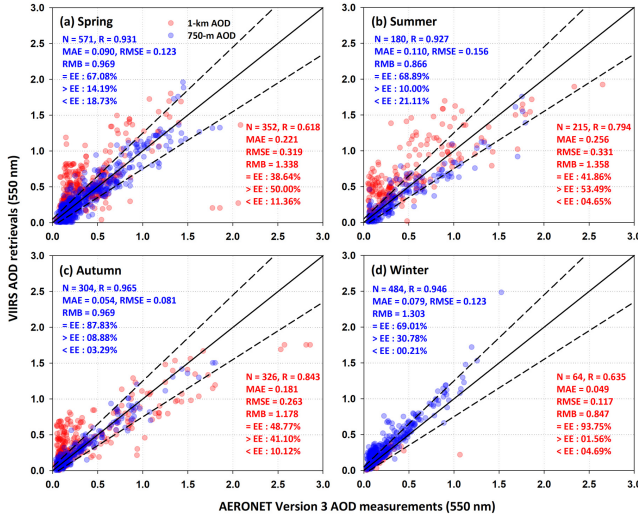


Fig. 5. Same as Fig. 4 but for different seasons. (a) Spring, (b) summer, (c) autumn, and (d) winter.

well and can benefit air pollution research over bright urban areas.

Over vegetated surfaces, the VAOOO AODs ($N = 269$) agree better with AERONET AOD measurements ($R = 0.876$) with an MAE of 0.122 and an RMSE of 0.214 [Fig. 4(b)]. Overall, more than 72% of the matchups fall within the EE envelope and the RMB is 0.898. The number of retrievals generated from our aerosol algorithm is increased by 57%. A similar fraction of these retrievals falls within the EE envelope (~76%). The correlation between our retrieved and AERONET-retrieved AODs is improved ($R = 0.924$), and the average MAE and RMSE values are reduced by 31% and 39%, respectively. These results suggest that our algorithm is overall better than the official aerosol algorithm over vegetated surfaces.

3) Comparison at the Seasonal Level: This section compares the overall performance between the two aerosol data sets at the seasonal level (Fig. 5). In spring [Fig. 5(a)], VAOOO AOD retrievals agree poorly with AERONET measurements with an MAE of 0.221 and an RMSE of 0.319. About 39% of the retrievals fall within the EE envelope. By contrast, there are 62% more successful retrievals generated from our algorithm, and they are better related to the AERONET AODs ($R = 0.931$) with lower estimation uncertainties (MAE = 0.09 and RMSE = 0.123). Approximately, 67% of the retrievals fall within the EE envelope.

Fig. 5(b) shows that similar poor performance with larger estimation uncertainty is seen for the official AOD product in summer. The retrievals are poorly correlated with AERONET measurements ($R = 0.794$) with a large MAE of 0.256 and an RMSE of 0.331. In general, 52% and 54% of the matched retrievals fall within and above the EE envelopes, respectively. By contrast, our retrievals show a higher correlation ($R = 0.927$) with ground measurements, with a lower MAE of 0.110 and an RMSE of 0.156, and a higher fraction of matched retrievals falling within the EE envelope (~69%).

Fig. 5(c) shows that autumnal VAOOO AOD retrievals generally agree better with AERONET AODs than those in

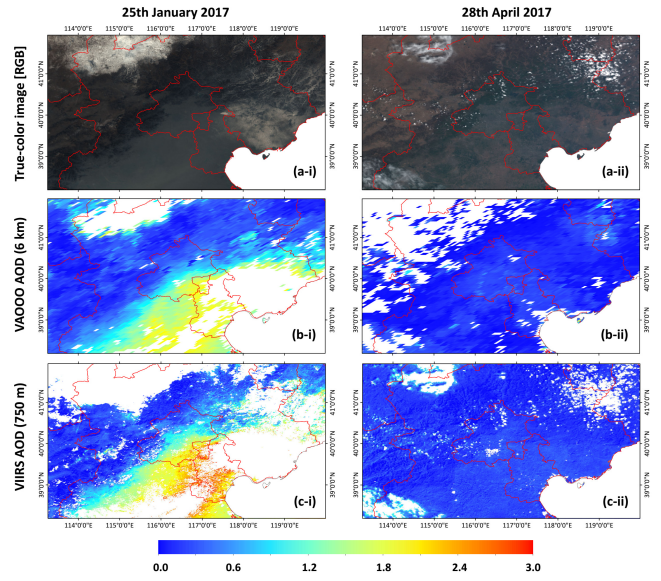


Fig. 6. Spatial distributions of VIIIRS (a) true-color (RGB) images, (b) VAOOO 6-km, and (c) our 750-m AOD retrievals in the study area.

spring and summer with a higher correlation ($R = 0.843$) and an overall decreasing estimation uncertainty (MAE = 0.181 and RMSE = 0.263). There are still some overestimations (RMB = 1.178), and only ~49% of the matched retrievals fall within the EE envelope. Our new AOD retrievals show the best performance in autumn among the four seasons and are an improvement over the official aerosol product with about 1.8 times more retrievals falling within the EE envelope, and MAE and RMSE values decreased by 70% and 69%, respectively.

In winter, VAOOO AOD retrievals show the lowest estimation uncertainty (i.e., MAE = 0.049 and RMSE = 0.117), and about 94% of them fall within the EE envelope [Fig. 5(d)]. However, only 64 matchups are collected from six sites, suggesting that the official algorithm is severely restricted in winter. However, our algorithm can better overcome this issue and generate 7.6 times more successful retrievals than the official algorithm. The matched retrievals correlate well with ground measurements ($R = 0.946$) with an MAE of 0.079 and an RMSE of 0.123. More than 69% of the retrievals fall within the EE envelope. These results illustrate that our proposed aerosol algorithm better captures the aerosol loadings in different seasons than does the official aerosol algorithm, especially in winter and spring. The main reason is that the underlying surface is relatively bright for exposing to nearly bare surfaces with less vegetation cover in winter. Meanwhile, the aerosol composition may change more due to dust or haze weather in spring. The better retrievals mainly contributed to the improvements in both the estimation of surface reflectance and the assumption of aerosol types.

C. Comparison in Spatial Distributions

Fig. 6 shows the true-color (RGB) images and spatial distributions of VAOOO 6-km and our 750-m AODs for a

high-aerosol-loading case on January 25, 2017 [Fig. 6(i)] and a low-aerosol-loading case on April 28, 2017 [Fig. 6(ii)], respectively. In general, the two aerosol data sets have similar AOD distributions, i.e., high aerosol concentrations in certain urban and low concentrations in the surrounding vegetated areas. However, there are noticeable differences in the spatial coverages of AOD. VAOOO AOD retrievals are always missing over bare land and urban areas to the northwest and central part of the study area. The main reason is that the official VIIRS aerosol algorithm involves the DT algorithm, and is thus severely limited in the applications over bright surfaces. However, our algorithm can better estimate the surface reflectance, leading to successful aerosol retrievals over such land surfaces. The official VIIRS aerosol algorithm also cannot accurately identify and mask the thin and broken clouds, resulting in spurious cloud-contaminated AOD retrievals. However, our algorithm with its more robust cloud detection scheme can generate more accurate AOD retrievals under these circumstances. Because of its eight times higher spatial resolution, our new data set can provide more detailed aerosol information than the official 6-km-resolution VIIRS AOD data set.

V. CONCLUSION

The objective of this study is to reduce uncertainty and improve the overall accuracy of the official VIIRS aerosol product. For this, a revised VIIRS aerosol retrieval algorithm, which is partly based on our previously proposed regionally RRHA algorithm for MODIS images, but is an extension with sufficient improvements, has been made to tackle three important challenges including modified VIIRS surface bidirectional reflectance, finer monthly aerosol type assumption, and an updated dynamic threshold cloud detection algorithm for VIIRS images. Then, the experiments are performed over the Beijing–Tianjin–Hebei region in Eastern China, which features severe air pollution problems and highly heterogeneous surfaces. The high-spatial-resolution (750 m) AOD retrievals from 2014 to 2017 are validated against AERONET measurements and also compared with the official VIIRS products.

The results show that our 750-m AOD retrievals are highly consistent with AERONET AOD measurements with small estimation uncertainties from site-specific to regional scales, indicating good data quality over both dark and bright surfaces. Meanwhile, the AOD retrievals are in good performance under different aerosol loadings, especially on highly polluted days. The data quality of the retrievals is significantly improved at urban sites. The official algorithm works poorly over bright surfaces, especially in winter with few successful retrievals. By contrast, our revised algorithm can better address this issue and improve the aerosol retrievals over bright surfaces. The spatial-distribution comparison can illustrate that our algorithm can provide more detailed information on aerosol loading over a greater spatial extent than the operational VIIRS algorithm as it is a more accurate cloud detection algorithm and a more robust aerosol algorithm. The revised VIIRS aerosol algorithm will thus be beneficial for aerosol studies, especially those focused on small-to-medium scales (e.g., urban areas).

ACKNOWLEDGMENT

The Visible Infrared Imaging Radiometer Suite (VIIRS) products are obtained from the NOAA Comprehensive Large Array-Data Stewardship System (<https://www.bou.class.noaa.gov>). The Moderate Resolution Imaging Spectroradiometer (MODIS) products are available from the NASA Earth Data Search (<https://search.earthdata.nasa.gov>). The Aerosol Robotic Network (AERONET) aerosol measurements are available from the NASA Goddard Space Flight Center, Greenbelt, MD, USA (<https://aeronet.gsfc.nasa.gov>).

REFERENCES

- [1] Y. J. Kaufman, D. Tanré, and O. Boucher, "A satellite view of aerosols in the climate system," *Nature*, vol. 419, no. 6903, pp. 215–223, 2002.
- [2] N. Bellouin, O. Boucher, J. Haywood, and M. S. Reddy, "Global estimate of aerosol direct radiative forcing from satellite measurements," *Nature*, vol. 438, pp. 1138–1141, Dec. 2005. doi: [10.1038/nature04348](https://doi.org/10.1038/nature04348).
- [3] R. J. Charlson *et al.*, "Climate forcing by anthropogenic aerosols," *Science*, vol. 255, no. 5043, pp. 423–430, 1992.
- [4] G. R. Carmichael *et al.*, "Asian aerosols: Current and year 2030 distributions and implications to human health and regional climate change," *Environ. Sci. Technol.*, vol. 43, no. 15, pp. 5811–5817, 2009.
- [5] L. Sun, J. Wei, D. H. Duan, Y. M. Guo, and X. T. Mi, "Impact of Land-Use and Land-Cover Change on urban air quality in representative cities of China," *J. Atmos. Sol.-Terr. Phys.*, vol. 142, pp. 43–54, May 2016.
- [6] Z. Li, D. Rosenfeld, and J. Fan, "Aerosols and their impact on radiation, clouds, precipitation & severe weather events," Oxford Res. Encyclopedias, Sep. 2017, pp. 1–36. [Online]. Available: <https://oxfordre.com/environmentalscience/view/10.1093/acrefore/9780199389414.001.0001/acrefore-9780199389414-e-126>. doi: [10.1093/acrefore/9780199389414.013.126](https://doi.org/10.1093/acrefore/9780199389414.013.126).
- [7] Z. Li *et al.*, "Aerosol and boundary-layer interactions and impact on air quality," *National Sci. Rev.*, vol. 4, pp. 810–833, Nov. 2017.
- [8] U. Pöschl, "Atmospheric aerosols: Composition, transformation, climate and health effects," *Angew. Chem. Int. Ed.*, vol. 44, no. 46, pp. 7520–7540, 2006.
- [9] Z. Li, F. Niu, J. Fan, Y. Liu, D. Rosenfeld, and Y. Ding, "Long-term impacts of aerosols on the vertical development of clouds and precipitation," *Nature Geosci.*, vol. 4, no. 12, pp. 888–894, 2011. doi: [10.1038/ngeo1313](https://doi.org/10.1038/ngeo1313).
- [10] Y. Wang, K.-H. Lee, Y. Lin, M. Levy, and R. Zhang, "Distinct effects of anthropogenic aerosols on tropical cyclones," *Nature Climate Change*, vol. 4, no. 5, pp. 368–373, 2014.
- [11] J. Wei, Y. Peng, R. Mahmood, L. Sun, and J. Guo, "Intercomparison in spatial distributions and temporal trends derived from multi-source satellite aerosol products," *Atmos. Chem. Phys.*, vol. 19, pp. 7183–7207, May 2019.
- [12] J. Wei *et al.*, "Estimating 1-km-resolution PM_{2.5} concentrations across China using the space-time random forest approach," *Remote Sens. Environ.*, vol. 231, Sep. 2019, Art. no. 111221. doi: [10.1016/j.rse.2019.111221](https://doi.org/10.1016/j.rse.2019.111221).
- [13] L. Sun *et al.*, "Aerosol optical depth retrieval over bright areas using Landsat 8 OLI images," *Remote Sens.*, vol. 8, no. 1, p. 23, 2016.
- [14] J. Wei, B. Huang, L. Sun, Z. Zhang, L. Wang, and M. Bilal, "A simple and universal aerosol retrieval algorithm for Landsat series images over complex surfaces," *J. Geophys. Res. Atmos.*, vol. 122, no. 24, pp. 13338–13355, 2017.
- [15] M. S. Wong, K.-H. Lee, J. E. Nichol, and Z. Li, "Retrieval of aerosol optical thickness using MODIS 500×500m², a study in Hong Kong and Pearl River delta region," *IEEE Trans. Geosci. Remote Sens.*, vol. 48, no. 8, pp. 3318–3327, Aug. 2010.
- [16] J. Wei and L. Sun, "Comparison and evaluation of different MODIS aerosol optical depth products over the Beijing-Tianjin-Hebei region in China," *IEEE J. Sel. Topics Appl. Earth Observ. Remote Sens.*, vol. 10, no. 3, pp. 835–844, Mar. 2017.
- [17] J. Wei *et al.*, "An improved high-spatial-resolution aerosol retrieval algorithm for MODIS images over land," *J. Geophys. Res. Atmos.*, vol. 123, no. 21, pp. 12291–12307, 2018.

- [18] J. Wei, Z. Li, Y. Peng, L. Sun, and X. Yan, "A regionally robust high-spatial-resolution aerosol retrieval algorithm for MODIS images over Eastern China," *IEEE Trans. Geosci. Remote Sens.*, vol. 57, no. 7, pp. 4748–4757, Jul. 2019. doi: [10.1109/TGRS.2019.2892813](https://doi.org/10.1109/TGRS.2019.2892813).
- [19] B. Ge *et al.*, "A dark target method for Himawari-8/AHI aerosol retrieval: Application and validation," *IEEE Trans. Geosci. Remote Sens.*, vol. 57, no. 1, pp. 381–394, Jan. 2018.
- [20] X. Yan *et al.*, "A minimum albedo aerosol retrieval method for the new-generation geostationary Meteorological Satellite Himawari-8," *Atmos. Res.*, vol. 207, pp. 14–27, Jul. 2018.
- [21] Z. Zhang *et al.*, "A simplified aerosol retrieval algorithm for Himawari-8 Advanced Himawari Imager over Beijing," *Atmos. Environ.*, vol. 199, pp. 127–135, Feb. 2019.
- [22] H. Zhang *et al.*, "An enhanced VIIRS aerosol optical thickness (AOT) retrieval algorithm over land using a global surface reflectance ratio database," *J. Geophys. Res., Atmos.*, vol. 121, no. 18, pp. 10717–10738, 2016.
- [23] A. M. Sayer, N. C. Hsu, J. Lee, C. Bettenhausen, W. V. Kim, and A. Smirnov, "Satellite ocean aerosol retrieval (SOAR) algorithm extension to S-NPP VIIRS as part of the 'deep blue' aerosol project," *J. Geophys. Res., Atmos.*, vol. 123, no. 1, pp. 380–400, 2018.
- [24] S. Shi *et al.*, "Multisensor data synergy of Terra-MODIS, Aqua-MODIS, and Suomi NPP-VIIRS for the retrieval of aerosol optical depth and land surface reflectance properties," *IEEE Trans. Geosci. Remote Sens.*, vol. 56, no. 11, pp. 6306–6323, Nov. 2018.
- [25] W. Wang, Z. Pan, F. Mao, W. Gong, and L. Shen, "Evaluation of VIIRS land aerosol model selection with AERONET measurements," *Int. J. Environ. Res. Public Health*, vol. 14, no. 9, p. 1016, 2017.
- [26] J. Zhu *et al.*, "Evaluation of aerosol optical depth and aerosol models from VIIRS retrieval algorithms over North China Plain," *Remote Sens.*, vol. 9, no. 5, p. 432, 2017.
- [27] L. He, L. W. Wang, A. Lin, M. Zhang, B. Muhammad, and J. Wei, "Performance of the NPP-VIIRS and Aqua-MODIS aerosol optical depth products over the Yangtze River Basin," *Remote Sens.*, vol. 10, no. 1, p. 117, 2018.
- [28] J. Wei, L. Sun, B. Huang, M. Bilal, Z. Zhang, and L. Wang, "Verification, improvement and application of aerosol optical depths in China Part 1: Inter-comparison of NPP-VIIRS and Aqua-MODIS," *Atmos. Environ.*, vol. 175, pp. 221–233, Feb. 2018.
- [29] Z. Li *et al.*, "Uncertainties in satellite remote sensing of aerosols and impact on monitoring its long-term trend: A review and perspective," *Annales Geophys.*, vol. 27, no. 7, pp. 2755–2770, 2009.
- [30] J. M. Jackson *et al.*, "Suomi-NPP VIIRS aerosol algorithms and data products," *J. Geophys. Res., Atmos.*, vol. 118, no. 22, pp. 673–689, Nov. 2013.
- [31] H. Liu *et al.*, "Preliminary evaluation of S-NPP VIIRS aerosol optical thickness," *J. Geophys. Res., Atmos.*, vol. 119, no. 7, pp. 3942–3962, Apr. 2014.
- [32] D. M. Giles *et al.*, "Advancements in the Aerosol Robotic Network (AERONET) Version 3 database—Automated near-real-time quality control algorithm with improved cloud screening for Sun photometer aerosol optical depth (AOD) measurements," *Atmos. Meas. Techn.*, vol. 12, pp. 169–209, Jan. 2019.
- [33] J. Wei, Z. Li, Y. Peng, and L. Sun, "MODIS Collection 6.1 aerosol optical depth products over land and ocean: Validation and comparison," *Atmos. Environ.*, vol. 201, pp. 428–440, Mar. 2019.
- [34] C. Schaaf and Z. Wang, "MCD43A1 MODIS/Terra+ Aqua BRDF/albedo model parameters daily L3 global–500 m V006," EOSDIS Land Processes DAAC, NASA, Washington, DC, USA, Tech. Rep., 2015. doi: [10.5067/MODIS/MCD43A1.006](https://doi.org/10.5067/MODIS/MCD43A1.006).
- [35] W. Wanner, X. Li, and A. H. Strahler, "On the derivation of kernels for kernel-driven models of bidirectional reflectance," *J. Geophys. Res., Atmos.*, vol. 100, no. D10, pp. 21077–21089, Oct. 1995.
- [36] J.-L. Roujean, M. Leroy, and P.-Y. Deschamps, "A bidirectional reflectance model of the Earth's surface for the correction of remote sensing data," *J. Geophys. Res., Atmos.*, vol. 97, no. D18, pp. 20455–20468, 1992.
- [37] W. Lucht, C. B. Schaaf, and A. H. Strahler, "An algorithm for the retrieval of albedo from space using semiempirical BRDF models," *IEEE Trans. Geosci. Remote Sens.*, vol. 38, no. 2, pp. 977–998, Mar. 2002.
- [38] X. Li and A. H. Strahler, "Geometric-optical bidirectional reflectance modeling of the discrete crown vegetation canopy: Effect of crown shape and mutual shadowing," *IEEE Trans. Geosci. Remote Sens.*, vol. 30, no. 2, pp. 276–292, Mar. 1992.
- [39] R. C. Levy *et al.*, "The collection 6 MODIS aerosol products over land and ocean," *Atmos. Meas. Tech.*, vol. 6, no. 11, pp. 2989–3034, 2013.
- [40] N. C. Hsu *et al.*, "Enhanced deep blue aerosol retrieval algorithm: The second generation," *J. Geophys. Res., Atmos.*, vol. 118, no. 16, pp. 9296–9315, Aug. 2013. doi: [10.1002/jgrd.50712](https://doi.org/10.1002/jgrd.50712).
- [41] J. Wei, Y. Ming, Q. Jia, and D. Yang, "Simple mineral mapping algorithm based on multitype spectral diagnostic absorption features: A case study at Cuprite, Nevada," *J. Appl. Remote Sens.*, vol. 11, no. 2, May 2017, Art. no. 026015.
- [42] L. Sun *et al.*, "A universal dynamic threshold cloud detection algorithm (UDTCDA) supported by a prior surface reflectance database," *J. Geophys. Res., Atmos.*, vol. 121, no. 12, pp. 7172–7196, Jun. 2016.
- [43] J. Wei, Z. Li, L. Sun, Y. Peng, and L. Wang, "Improved merge schemes for MODIS collection 6.1 dark target and deep blue combined aerosol products," *Atmos. Environ.*, vol. 202, pp. 315–327, Apr. 2019.



Jing Wei (S'16) received the M.E. degree in photogrammetry and remote sensing from the Shandong University of Science and Technology, Qingdao, China, in 2017. He is currently pursuing the Ph.D. degree in global environmental change with Beijing Normal University, Beijing, China.

He was a Research Assistant with the Chinese University of Hong Kong, Hong Kong, and also with Tsinghua University, Beijing. He has authored more than 60 papers. His research interests include the aerosol and cloud remote sensing, estimation of particulate matter concentrations, and aerosol–cloud–precipitation interactions.

Dr. Wei is an AGU Student Member.



Zhanqing Li received the B.Sc. and M.Sc. degrees from the Nanjing University of Information Science and Technology, Nanjing, China, in 1983 and 1989, respectively, and the Ph.D. degree from McGill University, Montreal, QC, Canada, in 1991.

He is currently a Professor with the University of Maryland, College Park, MD, USA. He has authored over 290 papers. His research interests include remote sensing, atmospheric physics, and climate and environment focusing on aerosol, cloud, radiation budget, and precipitation.

Dr. Li is a fellow of AMS, AGU, and AAAS. He received numerous awards in USA, Canada, and Germany. He is an Editor of the *Journal of Geophysical Research—Atmospheres*.



Lin Sun received the M.Sc. degree in meteorology from the Nanjing University of Information Science and Technology, Nanjing, China, in 2003, and the Ph.D. degree in cartography and geographic information system from the Institute of Remote Sensing and Digital Earth, Chinese Academy of Sciences, Beijing, China, in 2006.

He is currently a Professor with the College of Geomatics, Shandong University of Science and Technology, Qingdao, China. His research interests include cloud detection and aerosol retrieval from satellite data.



Yikun Yang received the M.E. degree in photogrammetry and remote sensing from Shandong University Science and Technology, Qingdao, China, in 2018. He is currently pursuing the Ph.D. degree in global environmental change with Beijing Normal University, Beijing, China.

His research interests include the retrieval and validation of land surface temperature and emissivity, aerosol, cloud microphysical parameters, and the aerosol–cloud–precipitation interactions.



Chuanfeng Zhao received the B.S. and M.S. degrees in atmospheric science from Peking University, Beijing, China, in 1999 and 2002, respectively, and the Ph.D. degree in meteorology from The University of Utah, Salt Lake City, UT, USA, in 2007.

He was a Post-Doctoral Researcher with the Lawrence Berkeley National Laboratory, Berkeley, CA, USA, and also with the Lawrence Livermore National Laboratory, Livermore, CA, USA, from 2007 to 2013. He is currently a Full Professor with Beijing Normal University, Beijing. His research interests include remote sensing and property retrieval of clouds, aerosol and precipitation, aerosol–cloud–radiation interaction, and anthropogenic pollution.



Zhaixin Cai received the M.Sc. degree from the Nanjing University of Information Science and Technology, Nanjing, China, in 2012. He is currently pursuing the Ph.D. degree in global environmental change with Beijing Normal University, Beijing, China.

His research interests include the cloud and precipitation physics, aerosol–cloud interaction, and air pollution.